2014

Detection of Seagrass Scars Using Sparse Coding and Morphological Filter

Ender Oguslu
Old Dominion University

Sertan Erkanli
Turkish Air Force

Victoria J. Hill
Old Dominion University, vhill@odu.edu

W. Paul Bissett
Florida Environmental Research Institute

Richard C. Zimmerman
Old Dominion University, rzimmerm@odu.edu

See next page for additional authors

Original Publication Citation

Oguslu, E., Erkanli, S., Hill, V., Bissett, W. P., Zimmerman, R., & Li, J. (2014). Detection of seagrass scars using sparse coding and morphological filter. In C.R. Bostater Jr., S.P. Mertikas, & Xavier Neyt (Eds.), *Remote Sensing of the Ocean, Sea Ice, Coastal Waters, and Large Water Regions 2014, Proceedings of SPIE Vol. 9240* (92400G) SPIE of Bellingham, WA. https://doi.org/10.1117/12.2069325

Detection of seagrass scars using sparse coding and morphological filter

Ender Oguslu[a,b], Sertan Erkanli[c], Victoria J. Hill[d], W. Paul Bissett[e], Richard C. Zimmerman[d] and Jiang Li[a]

[a]Department of Electrical and Computer Engineering, Old Dominion Univ., Norfolk, VA 23529
[b]Turkish Air Force NCO Vocational Collage, Gaziemir, Izmir, Turkey
[c]Turkish Air Force, Cankaya, Ankara, Turkey
[d]Department of Ocean, Earth and Atmospheric Sciences, Old Dominion Univ., Norfolk, VA 23529
[e]Florida Environmental Research Institute, Tampa, Florida 33611

ABSTRACT

We present a two-step algorithm for the detection of seafloor propeller seagrass scars in shallow water using panchromatic images. The first step is to classify image pixels into scar and non-scar categories based on a sparse coding algorithm. The first step produces an initial scar map in which false positive scar pixels may be present. In the second step, local orientation of each detected scar pixel is computed using the morphological directional profile, which is defined as outputs of a directional filter with a varying orientation parameter. The profile is then utilized to eliminate false positives and generate the final scar detection map. We applied the algorithm to a panchromatic image captured at the Deckle Beach, Florida using the WorldView2 orbiting satellite. Our results show that the proposed method can achieve >90% accuracy on the detection of seagrass scars.

Keywords: Remote sensing, sparse coding, scar detection, morphological filters.

1. INTRODUCTION

Seagrasses (marine angiosperms) inhabit the shallow coastal waters of temperate and tropical seas throughout the world. They provide critical habitat for a variety of wildlife, improve water quality, stabilize coastal sediments and represent an important reservoir of organic carbon (blue carbon) in the world ocean [1]. However, seagrasses are particularly vulnerable to human impacts in coastal environments that has created a global crisis in terms of their long-term sustainability [2]. Along heavily populated coasts, including the US Gulf of Mexico, mechanical damage from propeller scars caused by recreational boats operating in very shallow water can have significant impacts on seagrass distributions (Figure 1). It can take years for the scars to disappear, and they often accelerate further seagrass losses by facilitating erosion on the scar boundaries. Although remote sensing can provide an excellent tool for imaging propeller scars in shallow water, the detection and quantification of the scars has not been automated to enable rapid and reliable assessment of the damage they cause in coastal waters. There are many challenges for accurate scar detection. Although quasi-linear, scars can have different shapes ranging from straight lines to smooth curves to circles and ellipses. The scars can also have various lengths and widths that vary with seafloor bathymetry and age. Although scars are usually defined as bright quasi-linear regions surrounded by dark vegetation, the scars can appear as dark lines in very shallow water, particularly at low tide when adjacent seagrass leaves fill the depressions. All of these variations pose significant challenges for accurate scar detection.

One effective way to track the distribution of seagrasses scar is to use remote sensing surveys [3-5]. In [3], aerial photography of Charlotte Harbor, Florida, gathered in 1999 was used. First, delineation of scarred habitat polygons was performed using the ArcGIS 8.3 software. Then, an image analyst manually created three categories of scar polygons as light scarring, moderate scarring and severe scarring polygons. Finally, a map was generated showing the regions of light, moderate and severe scarred. Another similar project was performed in Gulf Coast of Texas with digital images captured with Leica ADS40 airborne digital camera in 2004 [4]. The significance of this project is that it is one of the first successful applications that utilized automated techniques for benthic habitat mapping. A recent study for mapping benthic habitat and identifying boat propeller scars in seagrass habitats compared the use of three digital airborne imagery, ADS40-52, DMC, and ULTRACAMD [5]. The images collected over Redfish Bay, Texas, were first brought into standard format in terms of radiometric, spectral, spatial resolutions for a fair comparison. To benefit from spectral

Remote Sensing of the Ocean, Sea Ice, Coastal Waters, and Large Water Regions 2014, edited by Charles R. Bostater Jr., Stelios P. Mertikas, Xavier Neyt, Proc. of SPIE Vol. 9240, 92400G
 · doi: 10.1117/12.2069325

and spatial resolutions, they created pansharpened images by using panchromatic and multispectral images of the region. It was concluded that the prop scars maps produced with ADS40-52 sensor were better than the maps produced by the other devices.

Figure 1. Examples of prop scar.

In this paper, we developed a pixel based two-step algorithm to detect the prop scars. In the first step, a set of features of scar and non-scar pixels were extracted by using the sparse coding method, which is a relatively new method developed for image processing tasks. Recent advances in sparse coding achieved state-of-the-art performances in many applications including image classification [6-8], and hyperspectral image (HSI) classification [9-10]. In sparse coding, a set of over-complete basis functions called a "dictionary" is learned from training data sets. Each data point is then projected onto the dictionary to obtain a new representation for the original data. After that, learning and classification are performed on the new representations. In our recent studies [11-12], we implemented a sparse coding method for HSI image classification and showed that randomly selected dictionaries can achieve good results making efficient HSI data classification possible. In this step, the sparse coding step classifies each pixel in the image as members of either scar or nonscar classes, generating an initial prop scar map.

In the second step, morphological directional filters [13-15] are applied to the classified scar pixels to eliminate false positives. Directional filters process an image in a defined direction to remove objects according to their orientations. In this work, "opening by reconstruction with a linear structuring element" [15] was used as the morphological filter. The operation of erosion followed by the operation of dilation is the so-called opening operation. The opening operation removes all objects which do not contain the specified structuring element (SE) with known shapes and sizes. The second step produces the final scar map. We applied the proposed algorithm to a panchromatic image collected in May 2010 near Deckle Beach, Florida, USA by WorldView2, an orbiting multispectral imaging system operated by DigitalGlobe, LLC. Our results showed that the method achieved >90% accuracy on the detection of seagrass scars, leading to an efficient scar detection system.

2. PROPOSED METHOD

Figure 2 shows the flowchart of the proposed method for scar detection. The proposed method consists of two main steps: (i) classification of the new features for pixels created using sparse coding to scar and nonscar categories, (ii) derivation of local orientation of each scar pixel to eliminate false positives and to produce the final scar map. Each step is detailed in the following subsections (Figure 2).

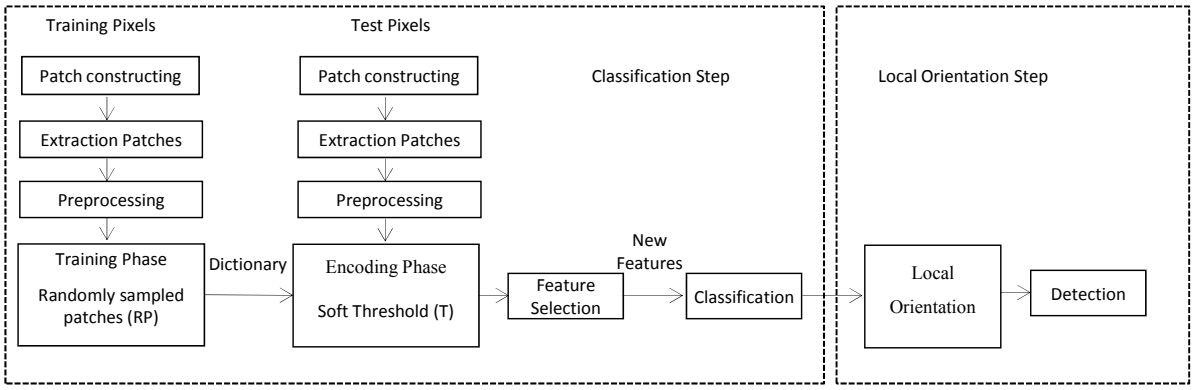

Figure 2. Flowchart of the proposed algorithm.

2.1 Classification of pixels to scar and nonscar using sparse coding

Patch extraction and dictionary learning from image

Training and test sets were constructed manually from the image. These sets made of scars, non-scars in land and non-scars in sea. First, the overlapped scar and non-scar blocks were created based on the middle point of the blocks. Each block was assigned to a scar-class if the middle point (pixel) of the block represented a scar. Otherwise, the block was assigned to the nonscar-class. The blocks were transformed into the vectors in dimension B representing the features of the pixel in middle point of each block.

After that, the patches were extracted in a similar style as we did in our previous works [11-12]. In particular, we randomly selected patches with a dimension of b-by-b from random blocks. Note that the extraction process is random and those extracted patches may overlap. The parameter "b" is often called "receptive field size". If m is the total number of sampled patches for dictionary learning, we denote it as $\mathbf{X}=\{x^{(1)}, x^{(2)}, ..., x^{(m)}\}$, where $x^{(i)} \in R^{bxb}$. Before the dictionary learning step, each patch $x^{(i)}$ was normalized to be zero mean and unit variance. X was then whitened by the zero-phase components analysis [16].

There are different types of dictionary learning methods in the literature such as k-means [17], orthogonal matching pursuit [18], sparse coding [7]. However, recent evidence suggests that random samples can achieve successful results in classification tasks [7] . It is simple and straight-forward in which the dictionary $\boldsymbol{D}$ is randomly picked from the extracted patches. The non-random methods are computationally expensive and rarely out-perform the random selection method.

Encoding and pooling

With the dictionary, $\boldsymbol{D}$, we obtained a new representation for a pixel as follows,

1. *Patch extraction*. We used a window of size b-by-b features to divide the blocks to patches. The window was moved along the block with a step size of '1', resulting in (B-b+1)-by-(B-b+1) patches for a block.
2. *Preprocessing*. These patches were preprocessed to make them zero mean, unit variance and whitened as described in the previous section.
3. *Encoding*. For each patch, we obtained a new representation by applying the soft thresholding technique as equation (1).

$$a^{(i)} = sign(z^{(i)})\max(0, \left|z^{(i)}\right| - t) \tag{1}$$

where t is an adjustable threshold, $z^{(i)}= \boldsymbol{D}^T \cdot x^{(i)}$ and *sign* is the mathematical function that extracts the sign of $(z^{(i)})$.

4. *Pooling*. We split all representations from (*B*-*b*+1)-by-(*B*-*b*+1) features of the block into *k* equal-sized groups and summed them in each group to obtain *k* representations. The final representation for each pixel is achieved by concatenating the *k* representations. The dimension of the final representation is *2kn*, where *n* is the number of basis function in the dictionary.

Feature selection and classification

After the encoding and pooling steps described above, the dimensionality of the new feature representation is 2*kn*. In our application, the dimensionality of the representation is still on the order of thousands that may be undesirable. We utilized the l_1/l_q regularized multi-class logistic regression [19-20] as shown in equation (2) to select effective features for the classification,

$$\min_{x} \sum_{l=1}^{k} \sum_{i=1}^{m} w_{il} \log(1+\exp(-y_{il}(w_l^T a_{il} + c_l))) + \lambda \|w\|_{l_1/l_q} \quad (2)$$

where a_{il}^T is the *i*-th feature for the *l*-th class, w_{il} is the weight for a_{il}^T, y_{il} is the response of a_{il}, c_l is the intercept (scalar) for the *l*-th class and λ is a regularization parameter. In this multiclass problem, a_{il}, $\forall l$, $A \in R^{m\text{x}n}$, $x \in R^{n\text{x}k}$, $c \in R^{1\text{x}k}$, $y \in R^{m\text{x}k}$. The l_1/l_q regularized regression optimization is a recently developed method that favors the group sparsity in the model [19-20]. Once we obtain the final representation vector for each pixel, we apply a weighted knn classifier [21] to sort the pixels into scar and non-scar classes. The regularization parameters of the logistic regression are determined by cross-validation.

2.2 Derivation of local orientation of scar pixel for false positive reduction

After the classification step, some unwanted objects (false positives) were also classified as scars. To remove the false positives, we computed local orientations of scar pixels using directional filters that defined morphological directional profile (MDP) for the pixel. The MDP of a pixel is the composition of outputs of the directional filter with a varying orientation parameter. We built the MDPs with "the opening by reconstruction with a linear structuring element". The MDP provides information about the orientation of the object due to the anti-extensivity property of the opening operators [13]. The anti-extensivity property means that the gray level of a pixel after the filtering is less than or equal to its original value. Thus, for a given orientation parameter, if the gray level of a pixel does not change, then the pixel belongs to an object where it is possible to fit a SE of size *L* and orientation θ. If the gray level decreased, then the pixel belongs to an object where it is not possible to fit the SE and orientation θ.

Two MDPs created with opening by reconstruction are shown in Figure 3. A scar generates a curved shape since the output of the directional filter changes as a function of the given orientation (Figure 3a). On the other hand, the shape of a non-scar is almost flat, since the output of the directional filter is the same regardless of the orientation (Figure 3b).

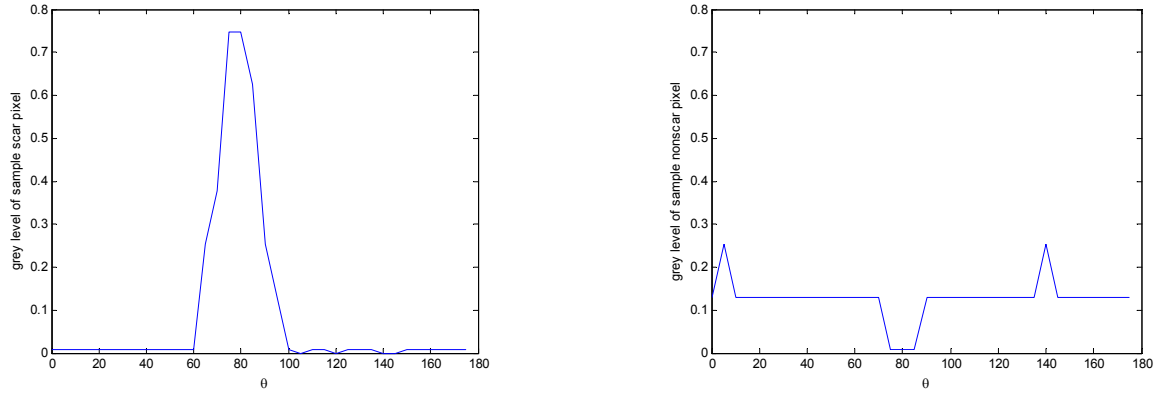

(a) (b)

Figure 3. MDPs created with opening by reconstruction.

Local spatial features can be extracted from the MDPs [22]. For a given pixel x the local orientation LO(x) is defined as the difference between the maximum value and the minimum value of the MDP:

$$LO(x) = \max_{\theta}\left(MDP(x)\right) - \min_{\theta}\left(MDP(x)\right) \tag{3}$$

From equation (3), if the pixel belongs to any oriented bright object, the local orientation will have a high value. On the contrary, if the pixel belongs to a non-oriented object the local orientation feature will have a very low value. In particular, local orientations of the scar pixels were obtained from the original image.

3. DATA PREPARATION AND PERFORMANCE EVALUATION

3.1 Data description

For this analysis, we used a part of a panchromatic image in May 2010 near Deckle Beach, Florida, USA by WorldView2, an orbiting multispectral imaging system operated by DigitalGlobe, LLC to evaluate our proposed method (Figure 4). The data has 0.33 m. spatial resolution and contains 2160 by 2160 pixels. Training and test sets were labeled manually. The labeled data set contains 1157 scar pixels, 447 non-scar pixels on land and 1161 non-scar pixels in the water. Some of scar pixels were shown in the red circles marked in the image.

To extract the feature from each pixel, we created a block of size 41 by 41 centered at the pixel. We assigned the block to scar class if the center pixel represents a scar. Otherwise, the block was assigned to nonscar class.

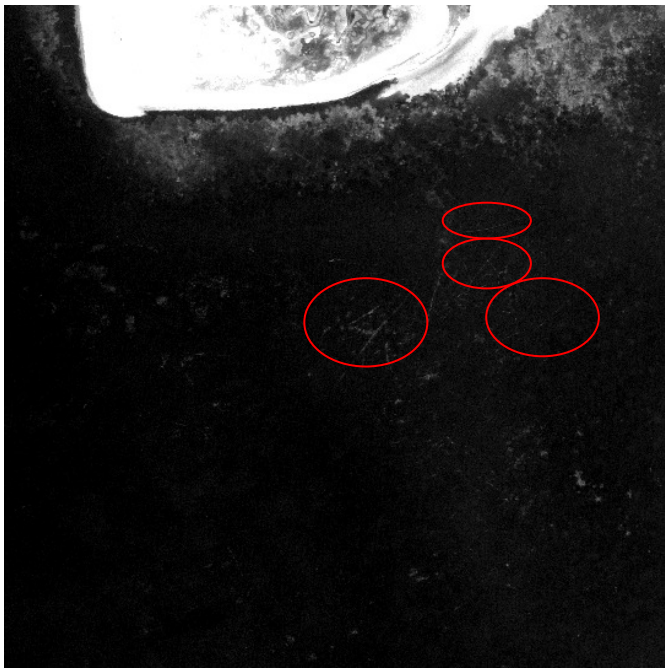

Figure 4. Test image.

3.2 Experimental setup and performance evaluation

In the experiment, we utilized 75% of all labeled data for training and the rest for testing. We repeated the experiment ten times and reported average performances of the ten runs. There were four parameters in the first step of the proposed method: (i) number of basis functions, n, (ii) group number in pooling, k, (iii) size of each patch called receptive field size, b, and (iv) threshold for encoding, t, in the coding step. In this study, we performed experiments many times and optimized those parameters.

The final scar detection was obtained by the second step based on local orientation information of scar pixels using a morphological filter called opening by reconstruction. The filter was tested with several linear structuring elements in different sizes. With those optimized parameters, we conducted our final experiment and reported our results in the next section.

4. RESULTS

4.1 Initial pixel classification results

Table 1 shows the classification results of the dataset using different number of nearest neighbor in the weighted knn algorithm [21]. In the experiment, the parameters of the proposed algorithm were set n= 500, k=10, b=20 and t=0.1. Before the feature selection step, there were about 10,000 features and the feature selection algorithm kept 2,000 of them.

It is clear that the proposed algorithm can fully detect the non-scars on land. However, some of the scar and non-scars features in the water were misclassified that the highest accuracy was achieved using 4-nearest neighbors.

Table 1. Classification results using different no. of nearest neighbor (%)

no. of nearest neighbor	1	2	3	4	5	6	7	8	9	10
Type of pixels										
Accuracy of non-scars in sea	87.2	87.6	88.2	88.4	88.3	88.3	88.2	88.1	87.9	87.8
Accuracy of non-scars in land	100	100	100	100	100	100	100	100	100	100
Accuracy of scars	90	91	91.5	92.1	92	92	91.8	91.8	91.5	91.4
Overall Accuracy	90.4	91	91.5	91.8	91.7	91.7	91.6	91.5	91.3	91.3

4.2 Visualization for the initial classification

We next applied the algorithm to the whole test image. All land cover pixels were assigned to non-scar category and there were many false positives in sea area (Figure 5).

Figure 5. Classification of test image.

4.3 False positive reduction based on local orientation

To remove the unwanted objects, local orientation of scar pixels of the classified test image were computed using the "opening by reconstruction" filter. The filter were tested with different structure element sizes (Figure 6). As observed in Figure 6(a) and 6(b), relatively small sizes of SE (15 and 30, respectively) did not remove the false positives. Most of the scars were kept while unwanted small objects were removed with the SE of length 30 (Figure 6(c)). Some large objects (nonscars) also remained and may represent rocks or other structural elements in sea. Increasing the SE size to 60 causes some thin scars to be missed (Figure 6d).

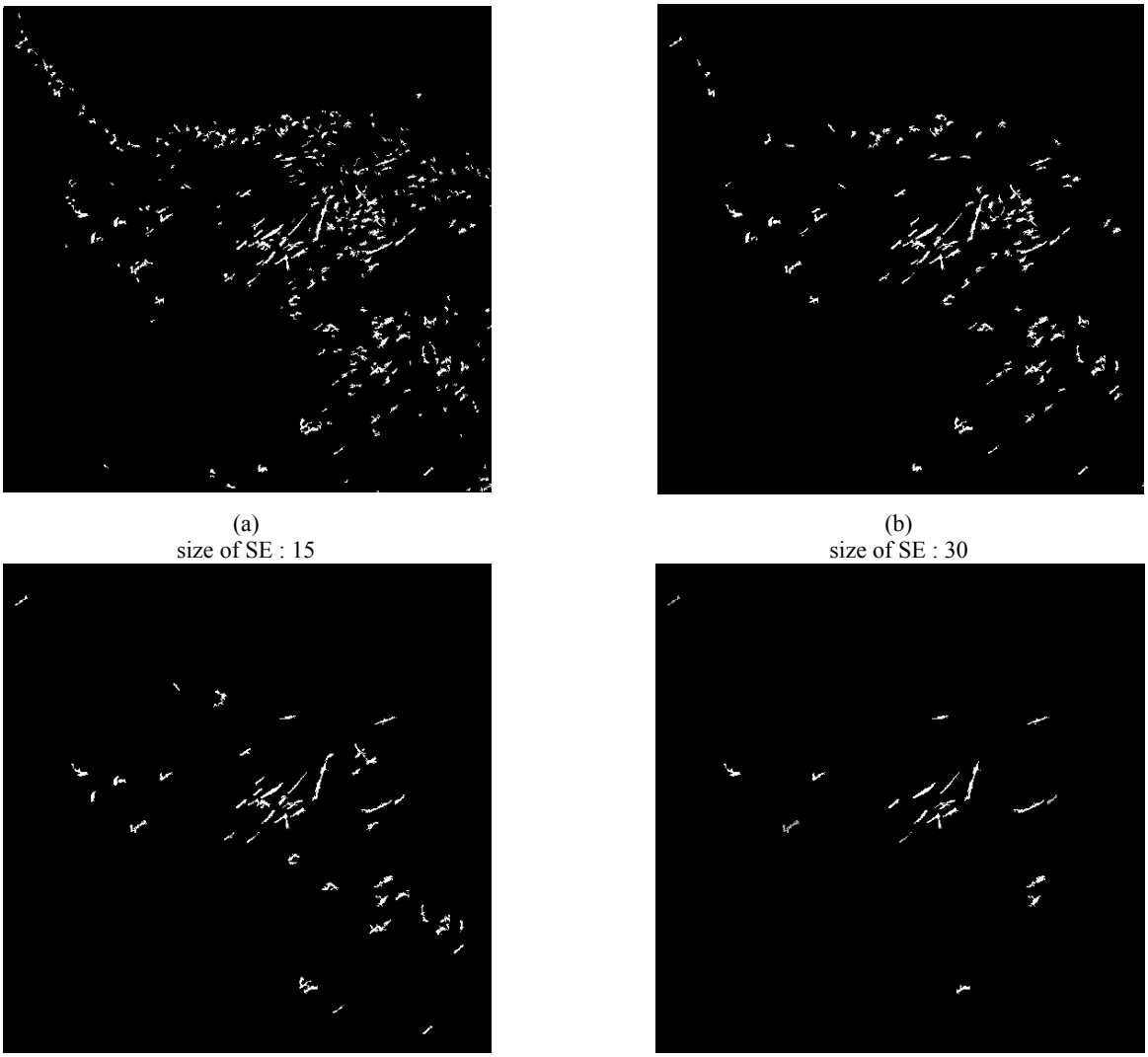

(a) size of SE : 15

(b) size of SE : 30

(c) size of SE : 45

(d) size of SE : 60

Figure 6. Mapping of scars.

5. CONCLUSION

Detection of propeller scars on seagrass beds has been addressed in this paper. We proposed a two-step straightforward and efficient algorithm for the detection of propeller seegrass scars using panchromatic image. The detection of the scars in classification step depends on the number of basis functions, group number in pooling, size of patches and threshold value. From the experimental results, we observed that this step can achieve >90% accuracy with those optimized parameters. However, false positive scar pixels are present due to brightness relative to adjacent areas in initial scar map. We utilized morphological directional profiles to eliminate false positives and generate the final scar detection map. The

size of linear SE is an important parameter to form the morphological directional profiles. Relatively small sizes of SE can still produce false alarm, which means that small formations of nonscar pixels are classified as scar pixels. Conversely, large sizes of SE cause some thin scars to be eliminated on final scar detection map. The optimized size of SE can keep the scars while remove the unwanted small objects. We also observed that some large objects (nonscars) also remained in the final scar map.

In this work, only spatial features of the pixels were used for detection of seagrass scars. Obviously, more features such as spectral features can be used to improve the detection of scars. This issue will be addressed in the future studies. We conclude that this promising algorithm could be implemented on a regular basis to monitor changes in habitat characteristics in coastal waters. It represents an important new capability for coastal management.

ACKNOWLEDGEMENT

Financial support for image acquisition was provided by the Florida Department of Environmental Protection, Office of Coastal and Management Areas under DEP Contract No. RM055.

REFERENCES

[1] Larkum, A., R. Orth, and C. Duarte, Seagrasses: Biology, Ecology and Conservation. Springer, Dordrecht, (2006)

[2] Orth, R., T. Carruthers, W. Dennison, C. Duarte, J. Fourqurean, K. Heck, A. Hughes, G. Kendrick, W. Kenworthy, S. Olyarnik, F. Short, M. Waycott, and S. Williams., "A global crisis for seagrass ecosystems." BioScience 56, 987-996 (2006).

[3] Blonski, Slawomir, "Spatial Resolution Characterization for QuickBird Image Products 2003-2004 Season," Proceeding of the High Spatial Resolution Commercial Imagery Workshop, (2004)

[4] Green K., Lopez C., "Using Object-Oriented Classification of ADS40 Data to Map the Benthic Habitats of the State of Texas," Photogrammetric Engineering and Remote Sensing 73(8), 861-864, (2007)

[5] Green K., Tukman M., Finkbeiner M., " Comparison of DMC, UltraCam, and ADS40 Imagery for Benthic Habitat and Propeller Scar Mapping," Photogrammetric Engineering & Remote Sensing, 589-599, (2011).

[6] J. Yang, K. Yu, Y. Gong and T. Huang, "Linear spatial pyramid matching using sparse coding for image classification," IEEE Conference on Computer Vision and Pattern Recognition, 1794-1801, (2009).

[7] Coates, A. Y. Ng and S. Mall, "The Importance of Encoding Versus Training with Sparse Coding and Vector Quantization," Proceedings of the 28th International Conference on Machine Learning (ICML), (2011).

[8] Gkioulekas and T. Zickler, "Dimensionality Reduction Using the Sparse Linear Model," Twenty-fifth Annual Conference on Neural Information Processing Systems (NIPS), (2011).

[9] S. Geman and D. Geman, "Stochastic relaxation, gibbs distributions, and the Bayesian restoration of images," IEEE Trans. Pattern Anal. Machine Intell, 6, (6), 721-741, (1982).

[10] Castrodad, Z. Xing, J. B. Greer, E. Bosch, L. Carin and G. Sapiro, "Learning discriminative sparse representations for modeling, source separation, and mapping of hyperspectral imagery," IEEE Trans. Geosci. Remote Sens., 49(11), 4263-4281, (2011).

[11] E. Oguslu, K. Iftekharuddin and J. Li, "Sparse coding for hyperspectral images using random dictionary and soft thresholding", Proc. SPIE 8399, 83990A, (2012).

[12] E.Oguslu, G.Zhou and J.Li, "Hyperspectral image classification using a spectral-spatial sparse coding model," SPIE Remote Sensing, 88920R-88920R-6, Dresden, Germany, (2013).

[13] M. Fauvel, B. Arbelot, J.A. Benediktsson, D. Sheeren and J. Chanussot, "Detection of Hedges in a Rural Landscape Using a Local Orientation Feature: From Linear Opening to Path Opening", Selected Topics in Applied Earth Observations and Remote Sensing, IEEE Journal of , 6(1), 15-26, (2013).

[14] P. Soille, Morphological Image Analysis: Principles and Applications, Second Edition, Springer, Berlin, (2003).

[15] P. Soille and H. Talbot, “Directional morphological filtering,” Pattern Analysis and Machine Intelligence, IEEE Transactions on, 23(11), 1313 -1329, (2001).
[16] Hyvarinen and E. Oja, “Independent component analysis: algorithms and applications,” Neural networks, vol. 13, (4-5), 411-430, (2000).
[17] Csurka G, Dance C, Fan L, Willamowski J, Bray C, "Visual categorization with bags of keypoints" Workshop on statistical learning in computer vision, ECCV 1 (1-22), (2004).
[18] Pati, Y. C., Rezaifar, R., and Krishnaprasad, P. S. “Orthogonal matching pursuit: recursive function approximation with applications to wavelet decomposition”, In Asilomar Conference on Signals Systems and Computers, (1993).
[19] Liu, S. Ji and J. Ye, "Multi-task feature learning via efficient L2,1-norm minimization", UAI, (2009).
[20] Guyon, J. Weston, S. Barnhill, and V. Vapnik, "Gene selection for cancer classification using support vector machines," Machine Learning, 46, (1-3), 389–422, (2002).
[21] Ma, M. M. Crawford and J. Tian, “Local manifold learning-based k-nearest-neighbor for hyperspectral image classification,” IEEE Trans. Geosci. Remote Sens. 48, (11), 4099-4109, (2010).
[22] P. Soille and M. Pesaresi, “Advances in mathematical morphology applied to geoscience and remote sensing,” IEEE Trans. Geosci. Remote Sens., 40, (9), 2042–2055, (2002).